

# Incommensurate magnetic structure of CeRhIn<sub>5</sub>

Wei Bao, P.G. Pagliuso, J.L. Sarrao, J.D. Thompson and Z. Fisk\*  
*Los Alamos National Laboratory, Los Alamos, NM 87545*

J. W. Lynn and R. W. Erwin

*NIST Center for Neutron Research, National Institute of Standards and Technology, Gaithersburg, MD 20899*  
 (May 29, 2018)

The magnetic structure of the heavy fermion antiferromagnet CeRhIn<sub>5</sub> is determined using neutron diffraction. We find a magnetic wave vector  $\mathbf{q}_M = (1/2, 1/2, 0.297)$ , which is temperature independent up to  $T_N = 3.8$  K. A staggered moment of  $0.374(5)\mu_B$  at 1.4 K, residing on the Ce ion, spirals transversely along the  $c$  axis. The nearest neighbor moments on the tetragonal basal plane are aligned antiferromagnetically.

CeRhIn<sub>5</sub> is a recently reported heavy Fermion compound that orders antiferromagnetically at  $T_N = 3.8$  K [1]. As a function of applied pressure, magnetism gives way to superconductivity with  $T_C = 2.1$  K at 16 kbar. Unlike the smooth evolution of  $T_N$  to zero reported for other Ce-based heavy-Fermion antiferromagnetic superconductors, e.g., CeIn<sub>3</sub> [2], in CeRhIn<sub>5</sub> the transition is apparently first-order [1]. CeRhIn<sub>5</sub> crystallizes in the tetragonal HoCoGa<sub>5</sub> structure ( $a = 4.65\text{\AA}$ ,  $c = 7.54\text{\AA}$  at 295 K), which can be viewed, at least schematically, as alternating layers of CeIn<sub>3</sub> and RhIn<sub>2</sub> [3]. It has been suggested that the resulting quasi-two-dimensional configuration of the CeIn<sub>3</sub> layers is at the heart of the unusual pressure dependence of CeRhIn<sub>5</sub>.

Magnetic susceptibility reveals a factor of two anisotropy at  $T_N$  for  $H \parallel c$  versus  $H \perp c$ . <sup>115</sup>In NQR measurements indicate that in the Néel state the ordered moments lie strictly in the CeIn<sub>3</sub> plane and suggest a spiral spin structure along the  $c$  axis [4]. The ordered moment develops much faster than would be expected in mean field theory and is inferred to saturate at about  $0.1\mu_B/\text{Ce}$ . Heat capacity [5] and NQR measurements [4] also point to a partial gapping of the Fermi surface coincident with the Néel transition that is suggestive of a spin-density-wave (SDW) state.

The magnetic behavior of CeRhIn<sub>5</sub> should be contrasted with that of CeIn<sub>3</sub>, which orders antiferromagnetically at 10 K. Neutron diffraction measurements reveal an ordered moment of  $0.48\text{--}0.65\mu_B/\text{Ce}$  and a commensurate ordering wave vector  $(1/2, 1/2, 1/2)$  [6,7]. The development of the ordered moment below  $T_N$  is consistent with mean field theory. The striking differences between CeIn<sub>3</sub> and CeRhIn<sub>5</sub> certainly suggest that a complete determination of the magnetic structure of the latter compound using neutron diffraction is indicated.

Single crystals of CeRhIn<sub>5</sub> were grown from an In flux as reported previously [1]. The resulting crystals are well-faceted rectangular parallelepipeds. Neutron scattering experiments were performed at NIST using the thermal triple-axis spectrometers BT9 with neutrons of energy  $E = 14.7$  meV, and BT2 with neutrons of  $E = 35$  meV. Pyrolytic graphite (PG) (002) was used as the monochro-

mator, as well as the analyzer when it was used in some scans. PG filters of 3 or 5 cm thickness were used to remove higher order neutrons. The horizontal collimations are 40-40-40-open at BT9 and 60-40-40-open at BT2. Sample temperature was regulated by a top loading pumped He cryostat. Lattice parameters at 1.2-7 K are  $a = 4.64\text{\AA}$  and  $c = 7.51\text{\AA}$ .

A powder sample, ground from 10 grams of crystals and inside a  $2.5 \times 5 \times 0.15$  cm Al container, was first examined at BT9. No peak showing temperature dependence between 1.2 and 7 K could be detected above the incoherent scattering background. This puts an upper limit for the intensity of any magnetic peak at 15% of that of the (100) structural peak.

A roughly disk-shaped single crystal of  $\sim 1$  cm in diameter and  $\sim 3$  mm in thickness, with the “disk” surface of the (001) plane, was used at BT9 to search for temperature dependent peaks. They were found as satellites of structural peaks with an incommensurate magnetic wave vector  $\mathbf{q}_M = (1/2, 1/2, \delta)$ . No higher order harmonics can be detected at  $2\mathbf{q}_M$  and  $3\mathbf{q}_M$ . The upper limits for them are 2% and 0.2% of the  $(1/2, 1/2, \delta)$  peak, respectively, at 1.6 K. Fig. 1(a) shows a pair of the satellite peaks and the incommensurability  $\delta = 0.297$ .

The intensity of the  $(1/2, 1/2, 0.297)$  Bragg peak is shown in Fig. 1(b) as the square of the order parameter of the magnetic phase transition. A Néel temperature of 3.8 K is consistent with that determined from heat capacity and resistivity [1]. The rapid development of the ordered moment with temperature is in agreement with the NQR measurements [4]. As shown by the scans at various temperatures in the insert to Fig. 1(b), there is no detectable change in the incommensurability,  $\delta$ , as a function of temperature. Additionally, there is no detectable broadening of the peak at this spatial resolution up to 3.6 K. In this regard, the incommensurate magnetic structure in CeRhIn<sub>5</sub> resembles that found in metallic  $V_{2-y}O_3$  [8] which is due to formation of a SDW by electrons on the nesting part of Fermi surface. However, the relation between the magnetic order parameter and resistivity for a SDW, observed in Cr and metallic  $V_{2-y}O_3$  [8,9], seems absent in CeRhIn<sub>5</sub> (refer to Fig. 3 in [1] and

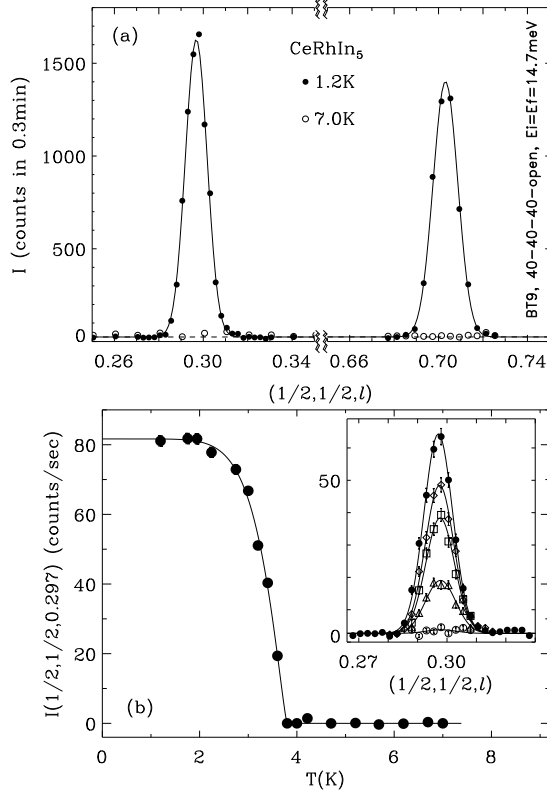


FIG. 1. (a) Elastic scan through a pair of magnetic Bragg points at 1.2 and 7 K. (b) Temperature dependence of the  $(1/2, 1/2, 0.297)$  Bragg peaks. Insert: Scans along the  $c$  axis, with decreasing intensity, at 3.0, 3.2, 3.4, 3.6 and 3.8 K.

Fig. 1(b) here).

The magnetic wave vector,  $\mathbf{q}_M = (1/2, 1/2, \delta)$ , already determines that the magnetic moments of Ce or Rh ions in an  $a$ - $b$  plane have a simple nearest-neighbor antiferromagnetic arrangement which changes incommensurately with a pitch  $\delta$  along the  $c$ -axis. This incommensurate change along  $c$ , in general, for magnetic moments at  $nc$ , takes the form

$$\mathbf{M} = M \operatorname{Re} [(\mathbf{x} + \alpha \mathbf{y}) e^{i 2\pi n \delta}], \quad (1)$$

where  $\alpha$  is a complex number,  $\mathbf{x}$  and  $\mathbf{y}$  are *any* two perpendicular unit vectors, and  $M$  is the magnitude of the magnetic moment. A trivial overall phase has been ignored here. To determine the remaining variables, a reasonable set of magnetic Bragg peaks needed to be measured.

To minimize significant absorption corrections associated with the large disk-shaped crystal, a bar-shaped single crystal of cross section  $\sim 1.5 \times 3$  mm in the scattering plane (sides along the  $c$  and  $(110)$  directions respectively) was measured at BT2 with neutrons of  $E = 35$  meV. At this energy, the neutron penetration length is 1.7 mm. A PG filter of 5 cm thickness is sufficient to suppress high order neutrons since an additional PG filter did

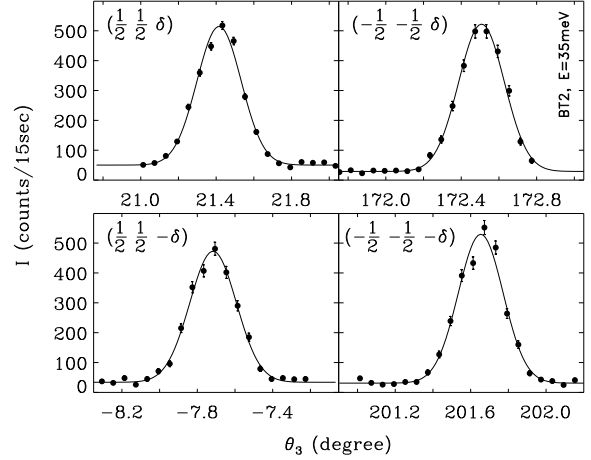


FIG. 2. Elastic rocking scans through magnetic Bragg points  $\{1/2, 1/2, 0.297\}$  at 1.4 K.

not change the intensity ratio among Bragg peaks  $(003)$ ,  $(220)$ ,  $(111)$  and  $(1/2, 1/2, 0.297)$ . Equivalent structural Bragg peaks, such as  $(111)$ ,  $(1\bar{1}\bar{1})$  and  $(\bar{1}\bar{1}\bar{1})$  with widely different rocking angles, have similar intensity, indicating that the sample is mostly transparent to the neutron beam.

Rocking scans for the quartet of the  $\{1/2, 1/2, 0.297\}$  magnetic Bragg peaks in Fig. 2 also show similar intensity. Besides reinforcing the rocking angle independence for Bragg peaks, the symmetry of these intensities places useful limits on the possible magnetic moment orientation.

Integrated intensities of 20 independent magnetic Bragg peaks were measured using rocking scans, such as those in Fig. 2. The scattering cross-sections,  $\sigma(\mathbf{q}) = I(\mathbf{q}) \sin(\theta_4)$ , normalized to structural Bragg peaks  $\{111\}$  to yield the absolute intensity, are listed in Table I. In such units,

$$\sigma(\mathbf{q}) = \left( \frac{\gamma r_0}{2} \right)^2 \langle M \rangle^2 |f(q)|^2 \sum_{\mu, \nu} (\delta_{\mu\nu} - \hat{\mathbf{q}}_\mu \hat{\mathbf{q}}_\nu) \mathcal{F}_\mu^*(\mathbf{q}) \mathcal{F}_\nu(\mathbf{q}), \quad (2)$$

TABLE I. Magnetic Bragg intensity, defined in Eq. (2), at 1.4 K in units of  $10^{-3}$  barns per  $\text{CeRhIn}_5$ .

$\mathbf{q}$	$\sigma$	$\mathbf{q}$	$\sigma$
$(0.5 0.5 0.297)$	8.9(2)	$(0.5 0.5 5.297)$	3.7(4)
$(0.5 0.5 0.703)$	10.8(2)	$(0.5 0.5 5.703)$	3.3(5)
$(0.5 0.5 1.297)$	13.2(2)	$(0.5 0.5 6.297)$	2.7(5)
$(0.5 0.5 1.703)$	12.6(1)	$(1.5 1.5 0.297)$	3.4(1)
$(0.5 0.5 2.297)$	11.0(1)	$(1.5 1.5 0.703)$	3.6(2)
$(0.5 0.5 2.703)$	9.5(1)	$(1.5 1.5 1.297)$	3.1(5)
$(0.5 0.5 3.297)$	7.7(2)	$(1.5 1.5 1.703)$	3.1(5)
$(0.5 0.5 3.703)$	6.8(5)	$(1.5 1.5 2.297)$	3.1(2)
$(0.5 0.5 4.297)$	6.3(7)	$(1.5 1.5 2.703)$	2.9(3)
$(0.5 0.5 4.703)$	5.9(8)	$(2.5 2.5 0.297)$	1.1(4)

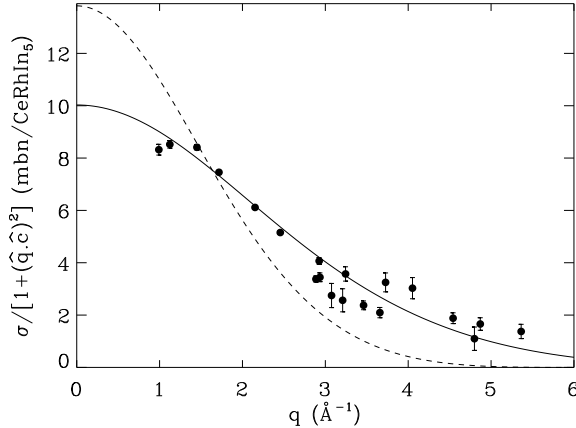


FIG. 3. The  $q$  dependence of magnetic cross-section,  $\sigma$ , divided by the polarization factor [refer to Eq. (3)]. The solid line is  $\text{Ce}^{3+}$  form factor [10], and the dashed line  $\text{Rh}^{+}$  form factor [11].

where  $(\gamma r_0/2)^2 = 0.07265 \text{ barns}/\mu_B^2$ ,  $M$  is the staggered moment,  $f(q)$  the atomic form factor,  $\hat{\mathbf{q}}$  the unit vector of  $\mathbf{q}$ , and  $\mathcal{F}_\mu(\mathbf{q})$  the  $\mu$ th Cartesian component of magnetic structure factor per  $\text{CeRhIn}_5$ .

The pattern of magnetic Bragg peaks (Table I and Fig. 2) indicates that  $\mathbf{z} \equiv \mathbf{x} \times \mathbf{y}$  is parallel to the  $c$  axis. We now consider two cases: (I)  $\alpha = \pm i$ , a magnetic spiral, and (II)  $\alpha = 0$ , a collinear magnetic moment modulation. For model I, the cross-section is

$$\sigma^I(\mathbf{q}) = \left(\frac{\gamma r_0}{2}\right)^2 \langle M \rangle^2 |f(q)|^2 (1 + |\hat{\mathbf{q}} \cdot \hat{\mathbf{c}}|^2). \quad (3)$$

For model II, let  $\mathbf{x} = \mathbf{a} \cos(\phi + \pi/4) + \mathbf{b} \sin(\phi + \pi/4)$ , i.e., magnetic moment pointing at an angle  $\phi$  away from the  $(110)$  direction in the  $a$ - $b$  plane. In general, there can be eight magnetic twins. Assuming equal occupation among the twins,

$$\sigma^{II}(\mathbf{q}) = \frac{1}{2} \left(\frac{\gamma r_0}{2}\right)^2 \langle M \rangle^2 |f(q)|^2 (1 + |\hat{\mathbf{q}} \cdot \hat{\mathbf{c}}|^2).$$

Thus  $\sigma^{II}(\mathbf{q}) = \sigma^I(\mathbf{q})/2$ , and model I and model II can not be distinguished in the diffraction. However, we prefer model I since a collinear magnetic modulation (model II) usually squares up with lowering temperature, generating higher order harmonics [12]. This is not what we have observed in  $\text{CeRhIn}_5$ . Handedness of the magnetic spiral ( $\alpha = i$  or  $-i$ ) can not be distinguished in this experiment.

Fig. 3 shows the quantity  $\sigma(\mathbf{q})/(1 + |\hat{\mathbf{q}} \cdot \hat{\mathbf{c}}|^2)$  which is proportional to atomic form factor  $|f(q)|^2$  [refer to Eq. (3)]. The  $\chi^2$  for best fit using  $\text{Rh}^{+}$  ion form factor (the dashed line) is one order of magnitude larger than that using the  $\text{Ce}^{3+}$  one (solid line). This indicates that the magnetic moments reside on the  $\text{Ce}$  ions rather than on the  $\text{Rh}$  ions. The staggered moment at 1.4 K is  $\langle M \rangle = 0.374(5)\mu_B$  per  $\text{Ce}$ .

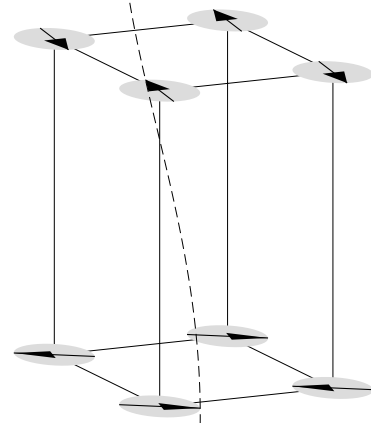


FIG. 4. Magnetic structure of  $\text{CeRhIn}_5$ . Only Ce sites are shown in the structural unit cell. The disk denotes the moment rotating plane. The dashed line traces the spiral.

Within a  $\text{CeIn}_3$  layer of  $\text{CeRhIn}_5$ , the local environment of a  $\text{Ce}$  ion is similar to that in the cubic compound  $\text{CeIn}_3$ . It is interesting to note that magnetic moments on these  $\text{Ce}$  share the same antiferromagnetic alignment. The twist of magnetic moments along the  $c$  axis in  $\text{CeRhIn}_5$ , approximately  $107^\circ$  per  $\text{CeIn}_3$  layer, apparently is related to the intervening  $\text{RhIn}_2$  layer. From this diffraction work, we cannot definitely tell whether this incommensurate twisting is due to competing magnetic interactions in a localized moment model or a divergent magnetic susceptibility at a nesting Fermi surface wave vector, i.e., a SDW. The staggered moment of  $0.374(5)\mu_B$  per  $\text{Ce}$  in  $\text{CeRhIn}_5$  is substantially reduced compared to that in its cubic counterpart  $\text{CeIn}_3$ . This could be a sign of SDW order, but could also be caused by a stronger Kondo effect or be a result of enhanced local moment fluctuations due to low dimensionality. Revealing evidences may be obtained in an inelastic neutron scattering experiment, as in the case of metallic  $\text{V}_{2-y}\text{O}_3$  [8,13].

In conclusion, we find the incommensurate magnetic structure as depicted in Fig. 4 for  $\text{CeRhIn}_5$ . A magnetic moment of  $0.374(5)\mu_B$  resides on the  $\text{Ce}$  ion at 1.4 K and the  $a$ - $b$  plane is its easy plane. Within an  $a$ - $b$  plane, magnetic moments form a simple nearest neighbor antiferromagnet on a square lattice, and they spiral transversely along the  $c$  axis with an incommensurate pitch  $\delta$ . The incommensurability,  $\delta$ , does not change with temperature.

We thank G. Aeppli, S. M. Shapiro, and C. Broholm for valuable discussions. Work at Los Alamos was performed under the auspices of the US Department of Energy. ZF gratefully acknowledges NSF support at FSU. PGP acknowledges FAPESP for partial support.

\* Permanent address: Florida State University, Tallahassee, FL 32306.

- [1] H. Hegger, C. Petrovic, E.G. Moshopoulou, M.F. Hundley, J.L. Sarrao, Z. Fisk, and J.D. Thompson, Phys. Rev. Lett. **84**, 4986 (2000).
- [2] N.D. Mathur, F.M. Grosche, S.R. Julian, I.R. Walker, D.M. Freye, R.K.W. Haselwimmer, and G.G. Lonzarich, Nature **394**, 39 (1998).
- [3] E.G. Moshopoulou, Z. Fisk, J. L. Sarrao and J. D. Thompson, submitted to J. Solid State Chem. (2000).
- [4] N.J. Curro, P.C. Hammel, P.G. Pagliuso, J.L. Sarrao, J.D. Thompson, and Z. Fisk, submitted to Phys. Rev. B (2000).
- [5] A.L. Cornelius, A.J. Arko, J.L. Sarrao, M.F. Hundley and Z. Fisk, submitted to Phys. Rev. B (2000).
- [6] J.M. Lawrence and S.M. Shapiro, Phys. Rev. B **22**, 4379 (1980).
- [7] A. Benoit, J.X. Boucherle, P. Convert, J. Flouquet, J. Palleau, and J. Schweizer, Solid State Commun. **34**, 293 (1980).
- [8] W. Bao, C. Broholm, S. A. Carter, T. F. Rosenbaum, G. Aeppli, S. F. Trevino, P. Metcalf, J. M. Honig and J. Spalek, Phys. Rev. Lett. **71**, 766 (1993).
- [9] D. B. McWhan and T. M. Rice, Phys. Rev. Lett. **19**, 846 (1967).
- [10] M. Blume, A. J. Freeman and R. E. Watson, J. Chem. Phys. **37**, 1245 (1962) .
- [11] P. J. Brown, page 451 in *International Tables for Crystallography*, Vol. C, Eds. J. C. Wilson and E. Prince, Kluwer Academic Publishers, Dordrecht, 1999 .
- [12] see, e.g., J. W. Lynn et al., Phys. Rev. B **55**, 6584 (1997).
- [13] W. Bao, C. Broholm, J. M. Honig, P. Metcalf and S. F. Trevino, Phys. Rev. B **54**, R3726 (1996).